Inflammation Research (2025) 74:2
https://doi.org/10.1007/s00011-024-01968-4

Inflammation Research

ORIGINAL RESEARCH PAPER

A universal gene expression signature-based strategy for the high-throughput discovery of anti-inflammatory drugs

Juan Feng[1,4] · Honglei Dang[3] · Xiaoling Zhang[2] · Wenting Huang[1,2] · Chengmei Ma[2] · Aixiang Zhang[2] · Mimi Hao[2] · Lan Xie[1,2]

Received: 16 September 2024 / Revised: 16 September 2024 / Accepted: 16 December 2024

Abstract

Background Traditional Chinese medicine (TCM) is a valuable resource for drug discovery and has demonstrated excellent efficacy in treating inflammatory diseases. This study aimed to develop a universal gene signature-based strategy for high-throughput discovery of anti-inflammatory drugs, especially Traditional Chinese medicine (TCM).

Methods The disease gene signature of liposaccharide-stimulated THP-1 cells and drug gene signatures of 655 drug candidates were established via sequencing. Anti-inflammatory drugs were screened based on similarities between drug gene signatures and the reversed disease gene signature.

Results Through screening, 83 potential anti-inflammatory drugs were identified. The efficacy of the TCM formula Biyun Powder, along with individual TCMs, *Centipedea Herba*, *Kaempferiae Rhizoma*, and *Schizonepetae Spica Carbonisata*, was verified in vitro or in vivo. Mechanistically, they exerted anti-inflammatory effects by inhibiting the nuclear factor-kappa B pathway. Kaempferol and luteolin were identified as bioactive IκB kinase-β inhibitors in *Kaempferiae* Rhizoma and *Schizonepetae Spica Carbonisata*, respectively.

Conclusion We developed a universal gene signature-based approach for the high-throughput discovery of anti-inflammatory drugs that is applicable to compounds and to TCM herbs/formulae and established a workflow (screening, validation of efficacy, and identification of the mechanism of action and bioactive compounds) that can serve as a research template for high-throughput drug research.

Keywords Gene signature · Anti-inflammatory drug discovery · Biyun Powder · *Centipedea Herba* · *Kaempferiae* Rhizoma · *Schizonepetae Spica Carbonisata*

Abbreviations

TC	Mtraditional Chinese medicine
LPS	Lipopolysaccharide
NF-κB	Nuclear factor-kappa B
TF	Transcription factor
IL-6	Interleukin-6
IL-1β	Interleukin-1 beta
IκB	Inhibitors of κB
CMAP	Connectivity map
HTS2	High-throughput sequencing-based high-throughput screening
RASL-seq	RNA-mediated oligonucleotide annealing, selection, and ligation with next-generation sequencing
COVID-19	Coronavirus disease 2019
DMSO	Dimethyl sulfoxide
GAPDH	Glyceraldehyde 3-phosphate dehydrogenase
LC-MS/MS	Liquid chromatography-tandem mass spectrometry
3D	Three dimensional
SD	Standard deviation

Communicated by John Di Battista.

✉ Lan Xie
xielan@tsinghua.edu.cn

[1] Medical Systems Biology Research Center, School of Medicine, Tsinghua University, Beijing 100084, China

[2] National Engineering Research Center for Beijing Biochip Technology, Beijing 102206, China

[3] Beijing CapitalBio Pharma Co., Ltd, Beijing 102206, China

[4] College of Health Science and Environmental Engineering, Shenzhen Technology University, Shenzhen 518118, China

Published online: 07 January 2025

PMA	Phorbol-12-myristate-13-acetate
DEGs	Differentially expressed genes
GSEA	Gene set enrichment analysis
NES	Normalized enrichment score
DEX	Dexamethasone
RT-qPCR	Realtime-quantitative polymerase chain reaction
BYP	Biyunsan, Biyun powder
CH	Bushicao, Centipedae Herba
MF	Xinyi, Magnoliae Flos
ARR	Xixin, Asari Radix et Rhizoma
CR	Chuanxiong, Chuanxiong Rhizoma
IN	Qingdai, Indigo Naturalis
KR	Shannai, Kaempferiae Rhizoma
Kae	Kaempferol
S. tenuifolia	Schizonepeta tenuifolia
SHC	Jingjietan, Schizonepetae Herba Carbonisata
SSC	Jingjiesuitan, Schizonepetae Spica Carbonisata
MPO	Myeloperoxidase
EGFP	Enhanced green fluorescent protein
MTC	Maximum tolerated concentration
dpf	days post-fertilization

Introduction

Inflammation is a vital defense mechanism used by a host to protect the body from various harmful stimuli and microbial invaders, such as pathogens, damaged cells, and chemicals [1]. However, when the inflammatory response fails to resolve certain persistent noxious stimuli in the body, e.g., the release of proinflammatory cytokines by adipose tissue, chronic inflammation occurs and causes systemic silent damage throughout the body [1]. Inflammation, especially prolonged chronic inflammation, is considered a major factor for the progression of various chronic diseases or disorders, including diabetes, cancer, cardiovascular diseases, arthritis, obesity, and autoimmune diseases [2]. Macrophages are key players in host defense against foreign pathogens. Stimuli such as lipopolysaccharide (LPS) activate macrophages, resulting in the production of proinflammatory cytokines and inflammatory mediators [3]. Nuclear factor-kappa B (NF-κB) is a heterodimeric transcription factor (TF) that typically contains p65 and p50 subunits, with the p65 subunit being considered the most important [4]. The NF-κB signaling pathway induces/regulates the expression of inflammatory mediators and inflammation-related genes, e.g., interleukin-6 (IL-6) and interleukin-1 beta (IL-1β), thereby playing critical roles in regulating inflammation [4]. The activation of NF-κB is closely associated with inhibitors of κB (IκB) family, which includes IκBα, IκBβ, and IκBε [5]. In the resting/normal state, NF-κB is present in the cytoplasm as an inactive complex with the inhibitor protein IκB. When activated by external stimuli such as LPS, IκBs are phosphorylated and degraded by the kinase IKKβ, leading to the translocation of the p65 subunit to the nucleus and increasing the transcription of various proinflammatory genes [5]. Overall, the NF-κB pathway is considered a popular target for anti-inflammatory drug development.

Various inhibitors against proinflammatory mediators are still being studied for use in the treatment of inflammatory diseases; however, their clinical use has been limited by severe side effects during pharmaceutical treatment [6, 7]. Traditional Chinese medicine (TCM) is a system of ancient medical practices that differs in methodology and philosophy from modern medicine and plays an important role in health maintenance in China. TCM formulae are increasingly favored in clinical settings because they are believed to cause few side effects. Therefore, screening TCM herbs/formulae with anti-inflammatory properties is highly important.

The gene expression signatures of cells or tissues can be used as "fingerprints" to define diseases [8]. Gene expression profiling of cellular perturbations has been used to effectively predict drug sensitivity [9] and the mechanism of action of compounds [10] and for quality control of TCMs [11], as well as for drug discovery [12]. Several gene expression signature-based high-throughput drug discovery approaches, such as the connectivity map (CMAP) platform, which includes transcriptomic profiles of thousands of compounds, and the high-throughput sequencing-based high-throughput screening (HTS^2) platform, which has been used to construct gene signatures of more than 8000 small molecules, have been developed [13]. HTS^2, which quantifies the expression of specific genes via RNA-mediated oligonucleotide annealing, selection, and ligation with next-generation sequencing (RASL-seq), has great advantages over other screening strategies in terms of throughput, automation, and cost [14]. Using HTS^2, we previously constructed the gene expression profiles of hundreds of TCMs to evaluate their immunomodulatory effects on coronavirus disease 2019 (COVID-19) [15, 16], to determine the mode of action of TCM formulae/herbs for treating cancer [17] and diabetes [18], and to develop new TCM formulae for the treatment of chronic heart failure [19].

In this study, we constructed gene expression profiles of more than 600 drugs in THP-1 cells and designed a strategy for the discovery of anti-inflammatory TCM/TCM formulae or compounds based on gene signature comparisons. In vitro and in vivo validation studies were conducted to confirm the reliability of the screening strategy. Finally, molecular docking was performed to identify bioactive components in

the TCMs. Overall, our study developed a reliable gene signature-based strategy and workflow for the high-throughput discovery of anti-inflammatory drugs.

Materials and methods

Cell culture and treatment

THP-1 monocytes and RAW264.7 murine macrophages were obtained from the National Infrastructure of Cell Line Resource (Beijing, China). All the cells were maintained at 37 °C in 5% CO_2 in a humidified atmosphere in RPMI 1640 medium (HyClone, Logan, UT) supplemented with 10% fetal bovine serum and 1% penicillin–streptomycin (HyClone).

Construction of a drug candidate bank

A total of 655 drug candidates, including 511 TCM herbs, 49 TCM formulae and 95 compounds (36 TCM ingredients and 59 clinically approved compounds), were subjected to screening. A list of all the drugs used is provided in Table S1. TCM herbs were purchased from Anguo Changda Chinese Herbal Pieces Ltd. (Hebei, China) and Beijing Tongrentang Medicine Corporation Ltd. (Beijing, China). Ten grams of TCM or TCM formula (prepared in specific ratios) was extracted and refluxed with 150 mL of 90% (v/v) ethanol for 3 h and concentrated for 20 min using a Soxhlet apparatus (BUCHI Labortechnik AG, Flawil, Switzerland). All the extracts were freeze-dried and dissolved in dimethyl sulfoxide (DMSO) at a concentration of 50 mg/mL, with some exceptions, as previously reported [16]. The test compounds were purchased from Selleck (Shanghai, China) or the National Institutes for Food and Drug Control (Beijing, China) and were prepared in DMSO at a stock concentration of 5 mM. JQ1 was utilized as a quality control among the batches. The plant names have been checked with http://www.theplantlist.org.

High-throughput RASL-seq experiments

To obtain the gene expression profiles of cells in response to drug candidates, high-throughput RASL-seq experiments were performed following a previously described protocol [16]. In brief, THP-1 cells (4,000 per well) were seeded in 384-well plates (Corning, Inc., Corning, NY) and incubated with 100 ng/mL phorbol-12-myristate-13-acetate (PMA) for 48 h, followed by treatment with TCM (formulae) crude extracts at 100 μg/mL or compound concentrations at 10 μM in triplicate for another 24 h. The cells were lysed and kept at -80 °C until the RASL assay was performed. The detected targets included 3267 genes related to virus infection, immunity, inflammation, metabolism, cell proliferation, apoptosis, and migration. Genes with a fold change greater than 1.5 and a p value less than 0.05 were identified as differentially expressed genes (DEGs).

RNA-seq experiment

THP-1 cells (15,000 cells per well) were seeded in 96-well plates (Corning, Inc., NY) in triplicate and incubated with 100 ng/mL PMA for 48 h, followed by stimulation with 1 μg/mL LPS (Escherichia coli O111:B4; Sigma–Aldrich, St. Louis, MO) for an additional 24 h. PMA-differentiated THP-1 cells in the absence of LPS stimulation were designated the control group. The cells were harvested, and RNA was isolated with TRIzol (Invitrogen, Carlsbad, CA). The libraries were constructed by using the Quick cDNA Library Preparation Kit (CapitalBio Corporation, Beijing, China) and sequenced on a HiSeq XTen system (Illumina, San Diego, CA). The RNA-seq data were mapped to the reference genome (hg19) by using HISAT2. The reads were counted, and StringTie was used to calculate the fragments per kilobase of exon model per million mapped fragments. The DEGs (fold change ≥ 2 and p value < 0.05) were identified by comparing the experimental group with the control group.

Strategy for anti-inflammatory drug screening by gene signature comparison

The similarity of gene signatures of the drug treatment groups (referred to as "drug signatures") with reversed disease gene signatures was calculated with a state-of-the-art signature search method proposed by Zhang et al. [20], which is abbreviated as SS_ZhScore analysis in the study by Tian et al. [21]. SS_ZhScore analysis is a simple and robust method for connecting drugs via unordered gene expression signatures by evaluating the consistency of the gene regulation status between the query list and the gene list of individual samples in the reference profile. It is described by the following equation [21]:

$$\mathrm{SS\_ZhScore} = \sum_{i=1}^{\mathrm{m}} R(gi) \times s(gi) \Big/ \sum_{i=1}^{m} (M - i + 1)$$

where gi represents the ith gene in the query gene list, $s(gi)$ is the signed rank (+1 for $\log_2$Fold change > 0 or -1 for $\log_2$Fold change < 0) in the query gene list, and $R(gi)$ is the signed rank of the gene in other samples influenced by different drugs. M and m are the lengths of R and s, respectively [21].

The SS_ZhScore calculation generates a list of drug candidates with normalized matching scores ranging from

+1 to -1, indicating the similarity of the input signature. A higher score indicates better similarity of the drug signature with the reversed disease signature, and a lower score indicates less similarity with the reversed disease signature. The R package fitdistrplus (https://github.com/aursiber/fitdistrplus) was subsequently used to fit the SS_ZhScore distribution for the drugs.

Cell viability assay

After RAW264.7 macrophages were seeded and grown in 96-well plates to 80% confluence, the cells were treated with different concentrations of drugs for 24 h, and DMSO was used as the vehicle control. The viability of the cells was subsequently assessed using a CCK-8 assay kit (Beyotime Biotechnology, Shanghai, China).

RNA isolation, cDNA synthesis, and realtime-quantitative polymerase chain reaction (RT-qPCR)

Total RNA was isolated with TRIzol reagent (Invitrogen) and purified with a TURBO DNA-free Kit (Invitrogen) according to the manufacturer's instructions. Total RNA (1 μg) was reverse transcribed into cDNA using a High-Capacity cDNA Reverse Transcription Kit (Thermo Fisher Scientific, Waltham, MA). RT-qPCR was conducted with the KAPA SYBR FAST qPCR Master Mix Kit (Kapa Biosystems, Woburn, MA) and a CFX Opus 96 Real-Time PCR System (Bio-Rad, Hercules, CA). Relative mRNA levels were determined by normalization to the level of the internal control gene glyceraldehyde 3-phosphate dehydrogenase (*GAPDH*) or *β-actin*. The relative gene expression data were analyzed using the ΔΔCT method. The sequences of primers used are listed in Table S2.

Liquid chromatography-tandem mass spectrometry (LC-MS/MS) analysis

High-resolution mass spectra were measured by a UPLC-Q-TOF/MS system (Waters, Milford, MA). A UPLC HSS T3 column (100×2.1 mm, 1.8 μm) was used for separation. The binary gradient of water containing 0.1% formic acid (v/v) (solvent A) and acetonitrile containing 0.1% formic acid (v/v) (solvent B) was applied at a constant flow rate of 0.25 mL/min at 35 °C with an injection volume of 1.0 μL. The linear gradient conditions were optimized as follows: 0–3 min, 0% B; 3–20 min, 0–20% B; 20–70 min, 20–100% B; 70–76 min, 100% B; and 76–80 min, 100-0% B. Samples were analyzed in both positive and negative ionization modes with scanning m/z ranging from 50 to 1500 Da. The instrumental settings of the LC-MS/MS were as follows: capillary voltage, 2.5 kV(-)/2.5 kV(+); cone voltage, 20 V (-)/40 V (+); source temperature, 125 °C (-)/120°C (+); and desolvation temperature, 400 °C (-)/650°C (+). The solvents were removed by evaporation under nitrogen at a flow rate of 800 L/h. Argon was used as the collision gas. The fragment ions were identified with the UNIFI TCM database (Waters).

IKKβ kinase activity assay

Cells in duplicate in 384-well assay plates were treated with different concentrations of compounds (0.1 μL), after which 5 μL of enzyme working solution was added to each well. After centrifugation at 1000 rpm for 1 min, the cells were incubated at 25 °C for 15 min. Then, 5 μL of substrate working solution was added, and the cells were incubated for 60 min at 25 °C. After another hour of incubation with ADP-Glo reagent, kinase detection reagent was added, and the cells were incubated for 60 min. Finally, the luminescence signal was measured for each well in a plate reader. The percentage of inhibition was calculated as follows: %inhibition = 100-(SignalCompound-Signalpositive control)/(Signalvehicle control-Signalpositive control)×100. Here, IKK16 was used as a positive control to inhibit IKKβ. All half-maximal inhibitory concentrations (IC50s) were calculated using %Inhibition with GraphPad Prism 6.0.

Molecular docking

The X-ray crystal structures of IKKβ (PDB ID: 4KIK) in complex with the inhibitor K-252a were downloaded from the Protein Data Bank. Pymol (version 2.5.0) [22] software was used for the pre-processing of the protein structure. The coordinates were chosen based on the location of K-252a ligand-binding pocket with coordinates and dimensions for X: 48.380, Y:30.005, Z:-56.761; X: 30, Y: 30, Z: 30. The ingredients of herbs were screened via TCMSP (http://lsp.nwu.edu.cn/tcmsp.php), TCMID (http://www.megabionet.org/tcmid/), and HIT2.0 (http://www.badd-cao.net:2345/). For each compound, three dimensional (3D) coordinates were generated via the ETKDG conformer generator implemented in the RDKit and minimized using the MMFF force field in the RDKit. All the compounds are docked into the active pocket of the IKKβ selected proteases to predict the binding poses for the selected compounds after grid box generating, ligand and protein preparations. Open Babel (v3.1.0) and AutoDock (v4.2.6) (https://ccsb.scripps.edu/) docking software were used for docking.

Zebrafish husbandry and studies

Wild-type AB strain zebrafish and transgenic myeloperoxidase (MPO): enhanced green fluorescent protein (EGFP)

strain zebrafish were provided by Suzhou Feifan Bio-technology Co. (Jiangsu, China). Zebrafish were kept at 28.5 °C with a 14:10-h light-dark cycle in a recirculating tank system using local tap water (pH 7.2–7.6, salinity 0.03–0.04%). Zebrafish naturally mating in pairs, and aged 3–5 days post-fertilization (dpf) were used for the experiment. The maximum tolerated concentration (MTC) of wild type AB zebrafish was determined in a preliminary experiment. In brief, a total of 180 wild-type AB zebrafish were randomly housed in a 6-well plate with 30 zebrafish each. Each well of zebrafish was given different dosages of tested drugs (125, 250, 500, 1000, or 2000 μg/mL) respectively for 48 h. The number of zebrafishes in each group was counted daily, and the dead zebrafish were promptly removed. To induce an inflammatory model, the yolks of AB zebrafish or transgenic MPO: EGFP zebrafish larvae were injected with 2 nL of 2 mg/mL LPS to induce inflammation. A negative control group was injected with PBS. Then, the inflammatory zebrafish were subjected to the test drugs by static immersion for 24 h. Ten transgenic zebrafish from each group were photographed under a fluorescence microscope. The images were analyzed using Image J software to analyze the number of neutrophils in the yolks of zebrafish larvae. For the RT-qPCR assay, wild-type AB zebrafish were treated as the MPO: GFP transgenic line. Total RNA was extracted from larvae of each group for determination of inflammatory cytokines via RT-qPCR. The whole experiment was in accordance with the Association for Assessment and Accreditation of Laboratory Animal Care International and was approved by the Animals Ethics Committee of Suzhou Feifan Bio-technology Co. (USTS2024017).

Data and statistical analysis

All the experimental results are presented as the mean ± standard deviation (SD), followed by paired (for in vitro study) or non-paired (for in vivo study) Student's t-test. Dose-dependence was analyzed via linear regression analysis. GraphPad Prism software 8.0 (San Diego, CA) was used for statistical analysis. Differences were considered significant if $p < 0.05$.

Results

Establishment of the gene expression signatures of the LPS-induced inflammatory cell model

Prior to screening for anti-inflammatory drugs, PMA-differentiated THP-1 cells were stimulated with LPS for 24 h to induce a cellular inflammatory response. We subsequently used RNA-seq to determine the LPS-triggered changes in gene expression at the transcriptional level in THP-1 cells. Analysis of the RNA-seq data revealed that LPS treatment resulted in 1832 DEGs, 872 of which were up-regulated, and 960 of which were down-regulated (Fig. 1A). Notably, the top up-regulated genes included several inflammation-related genes such as *CCL1*, *CCL19*, *TNF*, and *CXCL3* (Fig. 1A). Next, the detected genes were then subjected to KEGG pathway enrichment analysis via gene set enrichment analysis (GSEA). The effect of LPS stimulation on each pathway is represented by the normalized enrichment score (NES). A positive NES indicated that the pathway was enriched in up-regulated genes, and a negative NES indicated enrichment in down-regulated genes. As shown in Fig. 1B, the top 10 signaling pathways enriched in the LPS-regulated DEGs included "cytokine–cytokine receptor interaction", "TNF signaling pathway", "viral protein interaction with cytokine and cytokine receptor", "rheumatoid arthritis", "NF-κB signaling pathway", "influenza A", "inflammatory bowel disease", "legionellosis", "IL-17 signaling pathway", and "NOD-like receptor signaling pathway", which are related to inflammation and have positive NESs, indicating that a significant immune response occurred after LPS stimulation. Moreover, using DAVID, KEGG pathway enrichment analyses were also performed on the up-regulated and down-regulated genes respectively. Consistent with the GSEA results, inflammation-related pathways, including "cytokine–cytokine receptor interaction", "NOD-like receptor signaling pathway", "TNF signaling pathway" and "NF-κB signaling pathway", were significantly enriched in the LPS-induced up-regulated DEGs (Fig. 1C), whereas pathways such as "pathways in cancer" and "regulation of actin cytoskeleton" were enriched in the down-regulated DEGs (Fig. 1D). Overall, these results suggest that an inflammatory cell model was successfully constructed and that a typical inflammation-related gene signature was generated.

Establishment of drug-responsive gene expression profiles

A drug library composed of 655 drugs was constructed. The drug list included 511 TCM herbs recorded in the Chinese Pharmacopoeia (2020 edition, excluding those that were not commercially available or difficult to extract), 49 classical TCM formulae collected from the literature, and 95 compounds (36 TCM ingredients and 59 clinically approved compounds) (Table S1). High-quality high-throughput sequencing data of drug-responsive gene expression signatures were subsequently obtained via a series of unified experiments. Briefly, THP-1 monocytes were incubated with 100 ng/mL PMA for 48 h to induce differentiation into macrophages and then treated with the drug candidates for

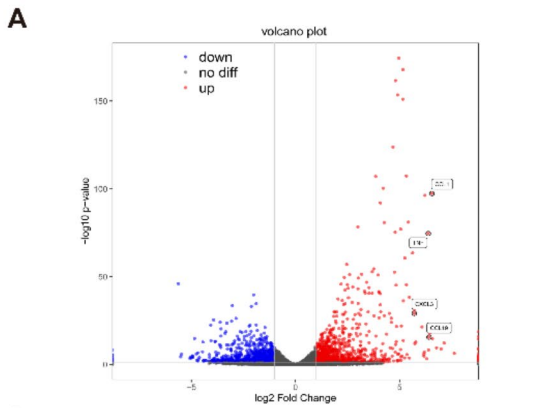

B

Rank	Pathway	NES	FDR
1	Cytokine-cytokine receptor interaction	3.57	0
2	TNF signaling pathway	3.03	0
3	Viral protein interaction with cytokine and cytokine receptor	3.22	0
4	Rheumatoid arthritis	2.75	8.38E-04
5	NF-kappa B signaling pathway	2.66	0.001
6	Influenza A	2.56	0.002
7	Inflammatory bowel disease	2.25	0.016
8	Legionellosis	2.19	0.018
9	IL-17 signaling pathway	2.19	0.019
10	NOD-like receptor signaling pathway	2.21	0.019

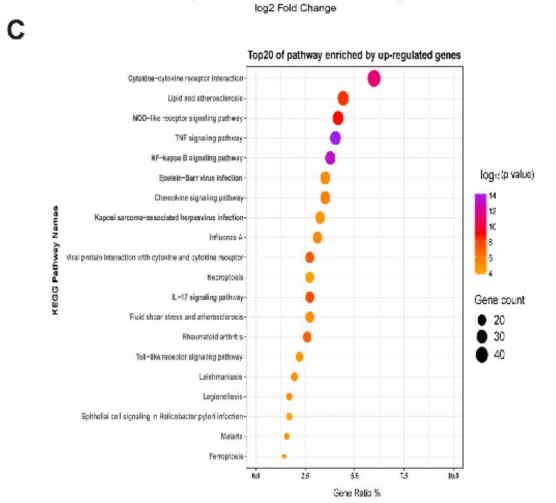

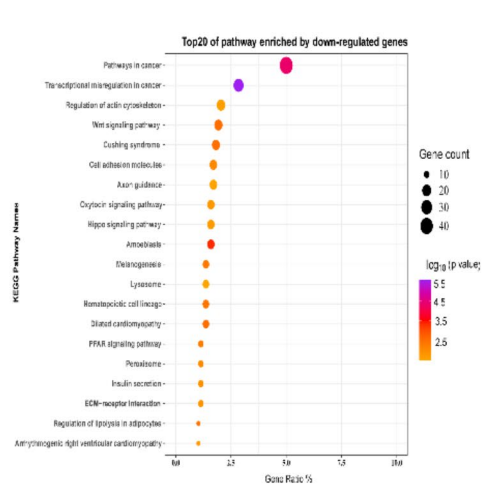

Fig. 1 Establishment of the gene expression signatures of the LPS-induced inflammatory cell model. **A** Volcano plot of DEGs induced by LPS. Red: up-regulated; Green: down-regulated. The cutoff was defined as a fold change ≥ 2 and $p < 0.05$. **B** The top 10 pathways enriched in DEGs induced by LPS via GSEA. NES: normalized enrichment score; FDR: false discovery rate. **C** The top 20 KEGG pathways enriched in genes up-regulated by LPS via DAVID. **D** The top 20 KEGG pathways enriched in genes down-regulated by LPS via DAVID

24 h. Then, the expression of 3267 genes derived from 139 pathways related to virus infection, immunity, inflammation, metabolism, cell proliferation, apoptosis, and migration was assessed via the standard pipeline as previously reported (Qiao et al., [16]. Finally, a compilation of high-throughput pharmaco-transcriptomic data of 655 drug candidates, namely, drug gene signatures, was constructed.

Gene signature-based high-throughput screening of anti-inflammatory drugs

Next, a high-throughput anti-inflammatory drug screening strategy was adopted on the basis of the gene signatures produced by LPS and drugs (referred to as the "disease signature" and "drug signature", respectively). First, a reverse disease signature was generated. The similarity of the drug signature with the reversed disease signature was subsequently calculated via SS_ZhScore analysis, a simple and

robust method for connecting drugs using unordered gene expression signatures [20]. This approach has been used to search for drugs for specific diseases or evaluate the transcriptomic expression similarities of samples influenced by different drugs [21]. To achieve unbiased comparisons, similarity analyses were conducted based on the expression profiles of 508 LPS-induced genes detected via RASL-seq. The ability of drugs to reverse LPS-induced gene expression disturbances was evaluated via the scaled SS_ZhScore (ranging from −1 to +1). A higher SS_ZhScore indicates greater similarity between the drug signature and the reversed disease signature, which also implies greater anti-inflammatory potential of drugs, and vice versa.

Among the 655 drug candidates, 291 had positive SS_ZhScore values ranging from +0.004 to +1, and 364 had negative SS_ZhScore values ranging from −1 to -0.004. The normal distribution and logistic distribution were subsequently used to analyze the SS_ZhScore distribution of the drugs. As the distribution plots show, the top 10% of drugs had an SS_ZhScore greater than 0.5 (Fig. S1). Therefore, we used 0.5 as the cutoff for the SS_ZhScore, namely, the top 10% to obtain anti-inflammatory drug candidates (the list of 83 drugs was provided in Table 1). JQ1, a bromodomain-containing protein 4 inhibitor first discovered as an antitumor agent, was subsequently confirmed to be an anti-inflammatory compound [23]. In this study, for the RASL-seq experiments, JQ1 was used as a quality control for each plate. As shown in Tables 1 and 7 JQ1 treated samples from different plates (7 plates in total) treated with JQ1 all had high SS_ZhScore values, ranging from 0.8 to 1, suggesting the reliability and stability of the screening strategy. In addition, dexamethasone (DEX), a glucocorticoid known as a potent clinical drug with anti-inflammatory effects [24] and, such as COVID 2019 [25], was also selected for screening. DEX ranked 7th with an SS_ZhScore value of 0.91 (Table 1). In addition to JQ1 and DEX, another clinically approved anti-inflammatory drug, mometasone furoate [26], was also identified as having anti-inflammatory effects in our screening, with an SS_ZhScore value of 0.81 (Table 1). Moreover, the screening results revealed that several compounds derived from TCMs are anti-inflammatory agents, such as kaempferol (SS_ZhScore: 0.96), resveratrol (SS_ZhScore: 0.82), apigenin (SS_ZhScore: 0.75), camptothecin (SS_ZhScore: 0.68), and curcumin (SS_ZhScore: 0.52) (Table 1), whose anti-inflammatory effects have been reported in previous studies by other groups [27–31]. TCMs such as *Cinnamomi Ramulus* (Guizhi, *Cinnamomum cassia* Presl, SS_ZhScore: 0.81) (Table 1), which has been reported to exert anti-inflammatory effects [32], were also effectively screened via this approach. The screening results also included several TCM prescriptions used to treat rhinitis in clinical practice, such as the Miao Medicine Compound Yu'e nasal drops (SS_ZhScore: 0.90), Biyun powder (SS_ZhScore: 0.81), Bining nasal spray (SS_ZhScore: 0.72), Biyanling tablets (SS_ZhScore: 0.72), and Qianbai Biyan tablets (SS_ZhScore: 0.67) (Table 1). Notably, the Mongolian medicine Xinkang capsule is a TCM preparation commonly used for the clinical treatment of coronary heart disease, angina pectoris, and hyperlipidemia. There are currently no studies reporting its anti-inflammatory effects; according to our screening, it has strong anti-inflammatory potential with a high SS_ZhScore of 1 (Table 1). Collectively, these results indicate that our approach can not only effectively identify known anti-inflammatory drugs but also screen new anti-inflammatory drugs.

Evaluation and validation of the anti-inflammatory activity of the TCM formula Biyun powder

To further verify the reliability and practicality of the screening strategy, we conducted several case studies to validate the anti-inflammatory activity of the selected drug candidates. Biyun powder (BYP, Biyunsan), a classic TCM formula used for the treatment of allergic rhinitis, is composed of five herbs, namely, *Centipedea Herba* (CH, Ebushicao, *Centipeda minima* (L.) A.Braun & Asch.), *Magnoliae Flos* (MF, Xinyi, *Magnolia biondii* Pamp.), *Asari Radix et* Rhizoma (ARR, Xixin, *Asarum heterotropoides* f. *mandshuricum* (Maxim.) Kitag.), *Chuanxiong* Rhizoma (CR, Chuanxiong, *Ligusticum striatum* DC.), and *Indigo Naturalis* (IN, Qingdai, *Baphicacanthus cusia* (Nees) Bremek.). According to our screening, the SS_ZhScore for the BYP (Biyunsan) group was 0.81, indicating its strong ability to reverse LPS-induced inflammation. Among the five TCM components, ARR (Xixin, 0.71), CH (Ebushicao, 0.52), and MF (Xinyi, 0.50) had positive scores, whereas CR (Chuanxiong, -0.32) and IN (Qingdai, -0.31) had negative scores, indicating that ARR (Xixin), CH (Ebushicao), and MF (Xinyi) are the main anti-inflammatory herbs in the formula. Furthermore, using DEX as a reference, we analyzed the correlations of the expression profiles of DEGs between the BYP (Biyunsan) formula and its component TCMs. As shown in Fig. 2A, the gene expression profile of the BYP (Biyunsan) treatment group was significantly positively correlated with the TCMs CH (Ebushicao), MF (Xinyi), ARR (Xixin) and even DEX; however, there was no correlation with CR (Chuanxiong) or IN (Qingdai) (Fig. 2A). Notably, CH (Ebushicao) presented the highest similarity to the BYP (Biyunsan) formula (Fig. 2A).

To further explore the reversing effects of BYP (Biyunsan) and its component TCMs on LPS-induced gene expression changes, the expression profiles of the LPS-regulated DEGs in each group were compared via hierarchical cluster analysis. The clustering analysis identified two large

Table 1 The list of drug candidates with a scaled SS_Zhscore greater than 0.5

No.	Drugs (English/Latin name)	SS_Zhscore
1	Mongolian Medicine Xinkang Capsules	1.00
2	JQ1	1.00
3	JQ1	0.98
4	Kaempferol	0.96
5	JQ1	0.96
6	JQ1	0.96
7	Dexamethasone	0.91
8	Shisanwei Honghua Pills	0.91
9	Miao Medicine Compound Yu'e Nasal Drops	0.90
10	Radxi Inula Cappa	0.88
11	JQ1	0.87
12	Trichosanthis Semen Tostum	0.85
13	JQ1	0.83
14	Resveratrol	0.82
15	Biyun Powder	0.81
16	Cinnamomi Ramulus	0.81
17	Mometasone Furoate	0.81
18	JQ1	0.81
19	Piperis Fructus	0.80
20	Zhenwu Decoction	0.79
21	Pyrrosiae Folium	0.78
22	Inulae Flos	0.77
23	Arnebiae Radix	0.76
24	Apigenin	0.75
25	Junci Medulla	0.75
26	Magnoliae Flos Kernels	0.75
27	Stellariae Radix	0.74
28	Saigae Tataricae Cornu	0.73
29	Bining Nasal Spray	0.72
30	Biyanling Tablets	0.72
31	Arisaematis Rhizoma Preparatum	0.71
32	Asari Radix Et Rhizoma	0.71
33	Siegesbeckiae Herba	0.70
34	Saussurea Lappa C. B. Clarke	0.69
35	Wangqi Nasal Drops	0.68
36	Bergeniae Rhizoma	0.68
37	Camptothecin	0.68
38	Schizonepetae Spica Carbonisata	0.68
39	Leonuri Herba	0.68
40	Qianbai Biyan Tablets	0.67
41	Artemisiae Argyi Folium	0.67
42	Scutellariae Radix	0.66
43	Aconitine	0.65
44	Vermilion	0.65
45	Kadsurae Caulis	0.65
46	Adriamycin	0.62
47	Vaccariae Semen	0.62
48	Polygoni Cuspidati Rhizoma Et Radix	0.62
49	Cinnamomi Cortex	0.62
50	Berberidis Radix	0.62
51	Sanziyangqin Decoction	0.61
52	Periplocae Cortex	0.61
53	Inulae Herba	0.61
54	Lygodii Spora	0.60
55	Notopterygii Rhizoma Et Radix	0.60

Table 1 (continued)

No.	Drugs (English/Latin name)	SS_Zhscore
56	Valerianae Jatamansi Rhizoma Et Radix	0.60
57	Eucommiae Cortex	0.60
58	Rhododendri Daurici Folium	0.60
59	Chrysanthemi Flos	0.59
60	Schizonepetae Herba Carbonisata	0.58
61	Chrysanthemi Indici Flos	0.57
62	Astragaloside Iv	0.57
63	Tranilast	0.57
64	Captopril	0.55
65	Capecitabine	0.55
66	Genkwa Flos	0.55
67	Atorvastatin Calcium	0.55
68	Piperis Longi Fructus	0.55
69	Iridis Tectori Rhizoma	0.55
70	Callicarpae Caulis Et Folium	0.55
71	Nelumbinis Receptaculum	0.55
72	Kaempferiae Rhizoma	0.55
73	Panacis Majoris Rhizoma	0.55
74	Dryopteridis Crassirhizomatis Rhizoma	0.54
75	Daturae Flos	0.54
76	Busulfan	0.53
77	Ginkgo Folium	0.53
78	Acarbose	0.52
79	Zhenwu Decoction	0.52
80	Realgar	0.52
81	Curcumin	0.52
82	Shaosha Qiwei Pills	0.52
83	Cirsii Japonici Herba Carbonisata	0.52
84	Centipedae Herba	0.52
85	Euodiae Fructus	0.52
86	Poriae Cutis	0.51
87	Nelumbinis Folium	0.51
88	Magnoliae Flos	0.50
89	Laggerae Herba	0.50
90	Notoginseng Radix Et Rhizoma	0.50

clusters: the first cluster included the LPS-stimulated group alone, whereas the second cluster contained the BYP (Biyunsan) formula and its five component TCMs (Fig. 2B). BYP (Biyunsan) had the greatest ability to reverse the LPS-induced gene interference (Fig. 2B). Three components, ARR (Xixin), MF (Xinyi), and CH (Ebushicao), also significantly reversed LPS-induced gene signatures, whereas the other two herbs, CR (Chuanxiong) and IN (Qingdai), showed little reversal (Fig. 2B), indicating that BYP (Biyunsan) has strong anti-inflammatory activity and that ARR (Xixin), MF (Xinyi), and CH (Ebushicao) are the main active anti-inflammatory herbs in the formula.

Network pharmacology analysis was subsequently conducted to investigate the mechanism underlying the anti-inflammatory activity of BYP (Biyunsan). A "formula-TCM-target-pathway" network was constructed (Fig. 2C). Degree values are commonly thought to be key indicators of the importance of nodes. CH (Ebushicao) had the greatest degree of correlation with the targets, followed by ARR (Xixin) and MF (Xinyi) (Fig. 2C), further confirming the importance of these components in the formulation. In addition, the core target genes were enriched in the NF-κB pathway, TNF signaling pathway, Toll-like receptor signaling pathway, etc. (Fig. 2C), indicating that BYP (Biyunsan) regulates multiple pathways and that the NF-κB pathway might play a significant role in the anti-inflammatory activity of BYP (Biyunsan). Therefore, TF enrichment analysis of DEGs regulated by BYP (Biyunsan) and one of its bioactive herbs, CH (Ebushicao), was carried out. The core TF NF-κB-p65 was indeed significantly enriched in the DEGs regulated by BYP (Fig. 2D) and the core bioactive herb CH (Ebushicao) (Fig. 2E). To visualize the results, heatmaps of the mRNA expression profiles of the DEGs with binding sites for NF-κB p65 were generated. The expression of

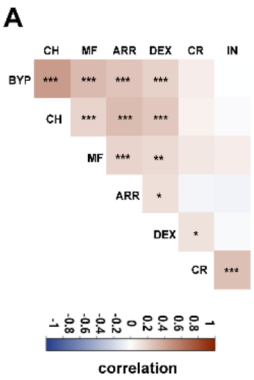

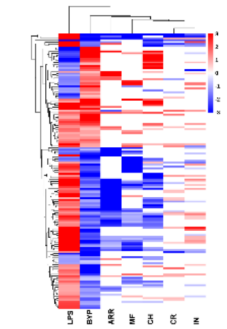

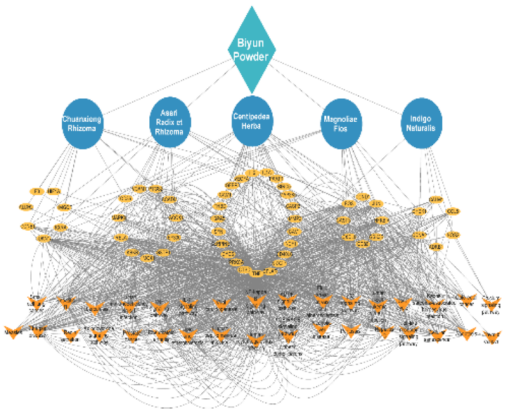

D

TF enrichment analysis of BYP-regulated genes		
Rank	Motif	Transcription Factor
1		NFκB-P65-REL(RHD)
2		SPIB(ETS)
3		PU.1(ETS)
4		HOXA13(HOMEOBOX)
5		ETSL-distal(ETS)

E

TF enrichment analysis of CH-regulated genes		
Rank	Motif	Transcription Factor
1		NFκB-P65-REL(RHD)
2		SPIB(ETS)
3		FRA2(bZIP)
4		HOXB13(HOMEOBOX)
5		ATF3(bZIP)

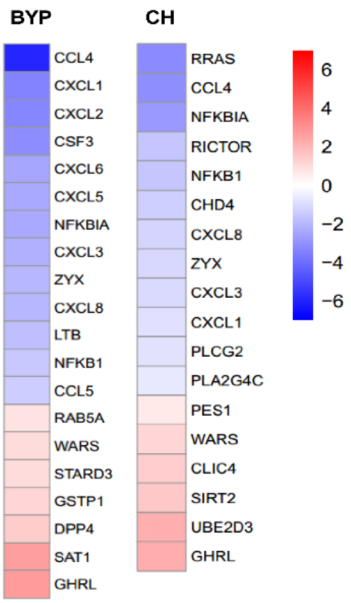

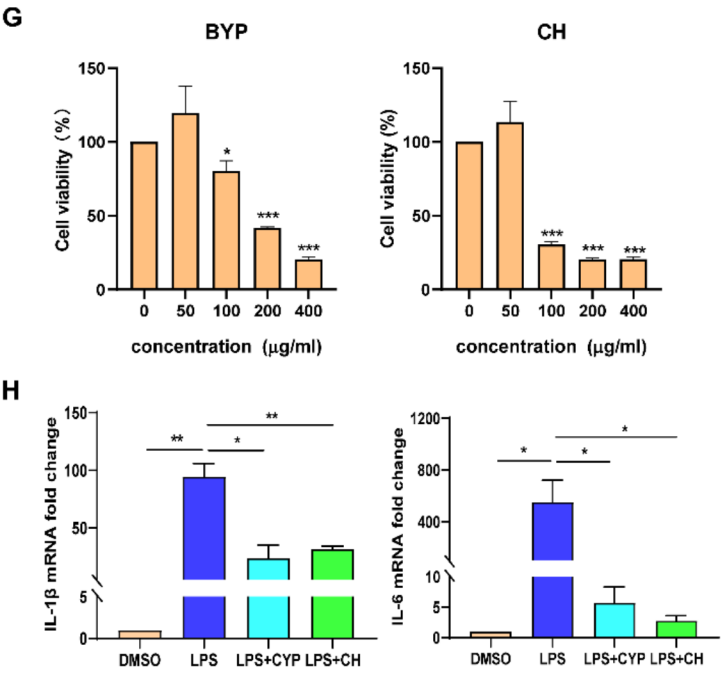

Fig. 2 Evaluation and validation of the anti-inflammatory activities of the TCM formula Biyun powder. **A** Pearson correlation analysis of the gene signatures of BYP and its four TCMs. **B** Heatmap showing the expression of DEGs induced by LPS in THP-1 cells treated with BYP and its component TCMs. **C** The "formula-TCM-target-pathway" network of BYP. **D** TF enrichment of genes regulated by BYP and **E** CH. **F** Heatmap representing the expression of NF-κB downstream genes in THP-1 cells treated with BYP and CH extracts. Red: up-regulated; blue: down-regulated. **G** Cell viability of RAW264.7 macrophages in response to treatment with different doses of BYP or CH extract. **H** RT–qPCR validation of the relative mRNA levels of *Il-1β* and *Il-6* in cells after treatment with BYP or CH extract. RAW264.7 cells were pretreated with BYP extract (100 μg/mL) or CH extract (50 μg/mL) for 1 h and then stimulated with 1 μg/mL LPS for another 24 h. $^{*}p<0.05$; $^{**}p<0.001$; $^{***}p<0.001$. $N=3$

proinflammatory genes regulated by NF-κB, such as *CCL4*, *CXCL1*, and *CXCL3*, was down-regulated by both BYP (Biyunsan) and CH (Ebushicao) (Fig. 2F). These results indicated that BYP (Biyunsan) and its bioactive TCM CH (Ebushicao) produce anti-inflammatory effects by inhibiting the NF-κB signaling pathway.

The anti-inflammatory effects of BYP (Biyunsan) and CH (Ebushicao) extracts were subsequently confirmed in RAW264.7 macrophages via RT-qPCR. Based on the changes in RAW264.7 cell viability induced by different doses of the CYP and CH extracts, as measured by CCK-8 assays (Fig. 2G), 100 and 50 μg/mL were selected as the working concentrations of the BYP (Biyunsan) and CH (Ebushicao) extracts, respectively. RAW264.7 cells were pretreated with BYP (Biyunsan) extract (100 μg/mL) or CH (Ebushicao) extract (50 μg/mL) for 1 h and then stimulated with 1 μg/mL LPS for another 24 h. The expression of two representative NF-κB-regulated genes, *Il-1β* and *Il-6*, was subsequently determined via RT–qPCR. As shown in Fig. 2H, both BYP (Biyunsan) extract and CH (Ebushicao) extract significantly down-regulated the LPS-induced expression of *Il-1β* and *Il-6*, confirming their ability to inhibit LPS-induced NF-κB-mediated inflammation.

Evaluation and validation of the anti-inflammatory activities of *Kaempferiae* Rhizoma and kaempferol

Kaempferiae Rhizoma (KR, Shannai), a traditional TCM herb derived from the medicinal plant *Kaempferia galangal* L., had an SS_ZhScore of 0.55 in the screening (Table 1). KR (Shannai) has a long history of use in the treatment of human diseases, including ailments such as cough and cold, fever, headache, rheumatic diseases, arthritis, and inflammation, and kaempferol is one of its major bioactive ingredients [33]. According to our screening, the flavonoid kaempferol was also found to be an anti-inflammatory agent with a high SS_ZhScore (0.96) (Table 1), second only to that of the Mongolian medicines Xinkang capsules and JQ1. Further correlation analysis revealed that the gene expression profiles of DEGs induced by KR (Shannai) extract and kaempferol were significantly positively correlated, and both were positively correlated with the gene signatures induced by DEX (Fig. 3A). Hierarchical cluster analysis revealed that both kaempferol and KR (Shannai) reversed the LPS-induced changes in gene expression (Fig. 3B), indicating that KR (Shannai) has an anti-inflammatory effect and that kaempferol is one of the bioactive constituents underlying this effect.

TF enrichment analysis revealed that the NF-κB p65 subunit was highly enriched among the genes regulated by the KR (Shannai) extract- and kaempferol (Fig. 3C,D). Consistently, heatmaps revealed that the expression levels of proinflammatory chemokines regulated by NF-κB, such as *CCL4*, *CXCL1*, *CXCL2*, and *CXCL3*, decreased greatly in response to KR (Shannai) extract and kaempferol treatment, supporting the inhibitory effects of KR (Shannai) extract and kaempferol on NF-κB-mediated inflammation (Fig. 3E). Therefore, it can be postulated that the herbal medicine KR (Shannai) and its bioactive ingredient kaempferol could inhibit inflammatory responses by blocking the NF-κB pathway.

Additionally, the anti-inflammatory effects of KR (Shannai) extract and kaempferol were verified in RAW264.7 macrophages. CCK8 assays revealed that lower doses (50 and 100 μg/mL) of KR (Shannai) extract were not cytotoxic and even promoted cell proliferation at 50 μg/mL (Fig. 3F). However, higher doses of KR (Shannai) extract (200 and 400 μg/mL) significantly reduced cell viability (Fig. 3F). Similarly, kaempferol was non-cytotoxic at doses of 10–50 μM but exhibited cytotoxicity at 100 μM (Fig. 3F). Therefore, safe doses of KR (Shannai) extract (100 μg/mL) and kaempferol (50 μM) were used for subsequent RT–qPCR assay. RT–qPCR analyses revealed that LPS stimulation significantly increased the expression of NF-κB downstream proinflammatory genes, while KR (Shannai) extract and kaempferol treatment effectively reversed the LPS-induced up-regulation of *Il-1β* and *Il-6* (Fig. 3G).

As mentioned above, the kinase IKKβ plays a central role in the activation of the NF-κB pathway by phosphorylating the inhibitor protein IκB, which leads to its degradation [5]. Therefore, we subsequently investigated whether kaempferol inhibits NF-κB pathway through the regulation of IKKβ. An in vitro IKKβ kinase activity assay demonstrated that kaempferol inhibited IKKβ activity, with an IC50 of 60.367 μM (Fig. 3H). Additionally, molecular docking simulations showed that kaempferol directly interacts with IKKβ at residues Leu21, Cys99, Glu61, Lys44, and Glu97 (Fig. 3I). Overall, our results suggest that KR (Shannai) extract inhibits LPS-induced NF-κB-mediated inflammatory responses and that kaempferol serves as a bioactive component by directly inhibiting IKKβ activity.

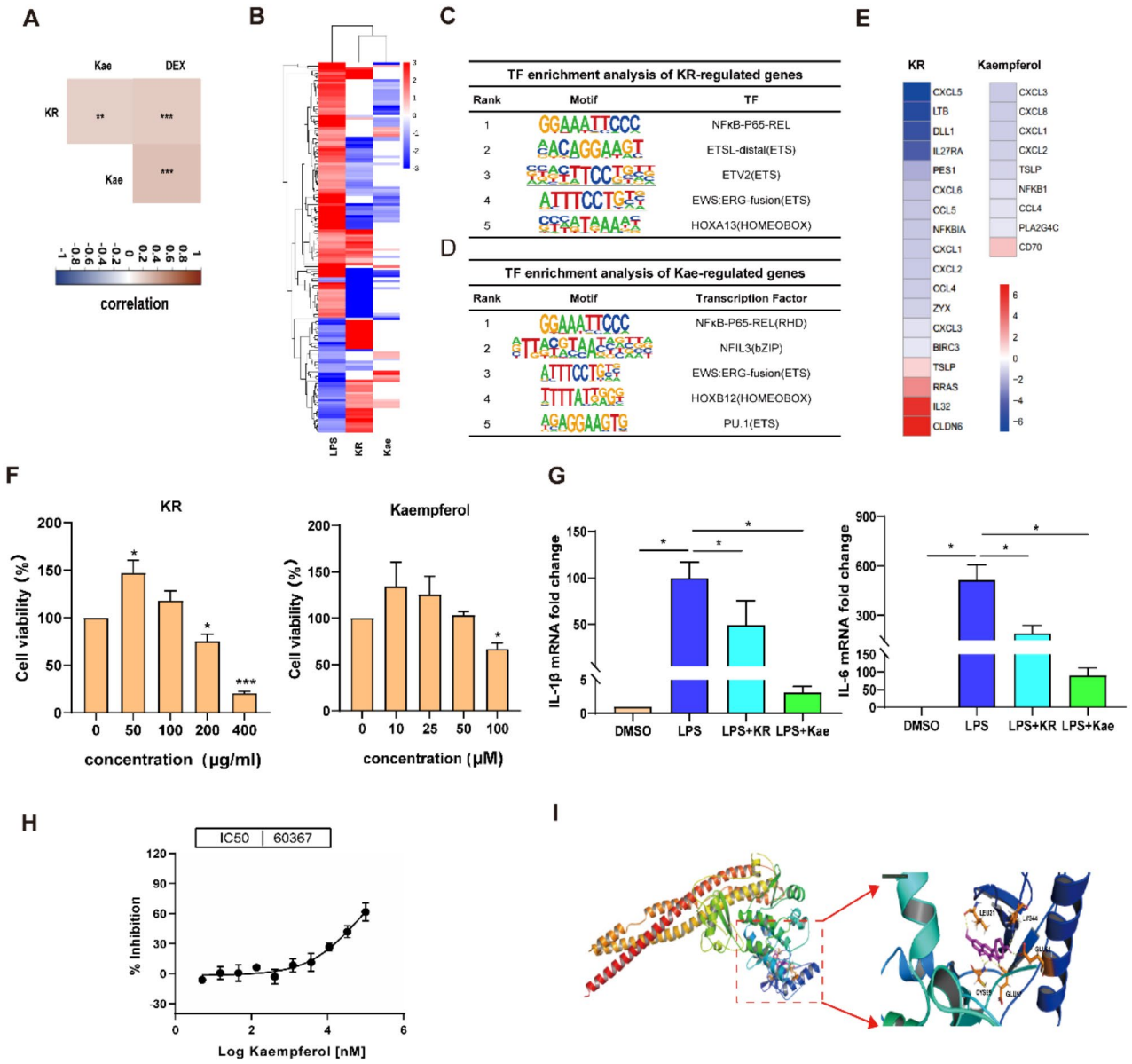

Fig. 3 Evaluation and validation of the anti-inflammatory activities of *Kaempferiae* Rhizoma and kaempferol. **A** Pearson correlation analysis of the gene signatures of the KR- and kaempferol-treated groups. **B** Heatmap representing the expression of DEGs induced by LPS in the LPS-, KR-, and kaempferol-treated groups. **C** TF enrichment of genes regulated by the KR extract and **D** kaempferol. **E** Heatmap showing the expression of NF-κB downstream genes after treatment with KR extract and kaempferol. Red: up-regulated; blue: down-regulated. **F** Cell viability of RAW264.7 macrophages in response to different doses of KR extract and kaempferol. **G** RT–qPCR validation of the relative mRNA levels of *Il-1β* and *Il-6* after treating cells with KR extract or kaempferol. RAW264.7 macrophages were pretreated with KR extract (100 μg/mL) or kaempferol (50 μM) for 1 h and then stimulated with 1 μg/mL LPS for another 24 h. **H** Effect of kaempferol on IKKβ activity. **I** Diagram of the computational docking between kaempferol and IKKβ (PDB ID: 4KIK). $*p<0.05$; $**p<0.001$; $***p<0.001$. $N=3$

Evaluation and validation of the anti-inflammatory activities of *Schizonepetae Spica Carbonisata*

Schizonepeta tenuifolia Briq. (*S. tenuifolia* Briq.), also known as Jing Jie in China, belongs to the Lamiaceae family and is a perennial herbaceous plant and an herbal medicine that has been widely used for thousands of years in China [34]. *Schizonepetae Herba Carbonisata* (SHC, Jingjietan) and *Schizonepetae Spica Carbonisata* (SSC, Jingjiesuitan) are processed with the dried aerial part and flower spike of *S. tenuifolia* Briq, respectively, by stir-frying until carbonization. SHC (Jingjietan) and SSC (Jingjiesuitan) are commonly used for treating hematochezia, metrorrhagia, and postpartum hemorrhage [35]. However, their anti-inflammatory activities remain largely unclear.

In our screening, SSC (Jingjiesuitan) ranked 9th with an SS_ZhScore of 0.68, while SHC (Jingjietan) had an SS_ZhScore of 0.58 (Table 1), indicating their anti-inflammatory activities. Pearson correlation analysis revealed a high correlation between the gene expression profiles of SHC (Jingjietan) and SSC (Jingjiesuitan), with both exhibiting a positive correlation with the anti-inflammatory drug DEX (Fig. 4A). LC-MS/MS analysis revealed similar chemical fingerprint spectra for SHC (Jingjietan) and SSC (Jingjiesuitan) (Fig. S2A), comparable chemical profiles between these two herbs. Additionally, hierarchical cluster analysis demonstrated that both SHC (Jingjietan) and SSC (Jingjiesuitan) extracts effectively reversed LPS-induced changes in gene expression (Fig. 4B).

TF enrichment analyses of DEGs regulated by these two herbs were subsequently performed. Notably, the NF-κB p65-REL motif was most significantly enriched in the genes regulated by SHC (Jingjietan) and SSC (Jingjiesuitan) (Fig. 4C&D). The expression heatmap of genes enriched in the NF-κB p65-REL motif revealed that NF-κB downstream proinflammatory genes, such as *CXCL1-3*, were dramatically downregulated by SHC and SSC (Fig. 4E). These results indicate that SHC and SSC have inhibitory effects on NF-κB-mediated inflammation. Next, using SSC as an example, we verified its anti-inflammatory activity in RAW264.7 macrophages. First, CCK-8 assays were performed to evaluate its effect on cell viability. The results revealed that 50 and 100 μg/mL SSC (Jingjiesuitan) extract had no cytotoxic or even protective effects on cell viability. However, when the dose increased to 200–400 μg/mL, the SSC (Jingjiesuitan) extract impaired cell viability in a dose-dependent manner ($R^2 = 0.99$, $p < 0.001$ for the linear regression curve, Fig. 4F). Therefore, 100 μg/mL SSC (Jingjiesuitan) extract was used for subsequent RT–qPCR assays. RT–qPCR validation experiments revealed that SSC (Jingjiesuitan) decreased LPS-stimulated *Il-1β* and *Il-6* expression (Fig. 4G).

Owing to their unique advantages in that their pathological features in terms of inflammation are similar to those of humans, zebrafish have been established as ideal models to study the pathophysiology of human inflammatory-related diseases [36]. Therefore, an LPS-induced zebrafish inflammatory model was used to assess the in vivo anti-inflammatory activity of SSC (Jingjiesuitan). Based on the MTC results (Fig. S2B; Table S3), SSC (Jingjiesuitan) extract was administered at three dosages: low (500 μg/mL), medium (1000 μg/mL), and high (2000 μg/mL), with DEX (2000 μg/mL) serving as the positive control. First, the effect of SSC (Jingjiesuitan) on LPS-induced neutrophil recruitment was examined using the MPO: EGFP transgenic zebrafish line, which allows live tracking of neutrophils. Zebrafish at 3 dpf were injected with 2 nL of LPS (2 mg/mL) into the yolk to induce inflammation, while the control group received an equal volume of PBS. The LPS-injected zebrafish were then immersed in DEX (2000 μg/mL), or three different dosages of SSC (Jingjiesuitan) extract for 24 h. Compared to the control group, larvae of the LPS-injected group exhibited massive neutrophil recruitment in the yolk, which was significantly reduced by SSC (Jingjiesuitan) in a dose-dependent manner ($R^2 = 0.67$, $p < 0.001$ for the linear regression curve, Fig. 4H,I). Then the effects of SSC (Jingjiesuitan) extract on the expression of inflammatory cytokines were investigated in the LPS-injected wild-type zebrafish. The mRNA expression levels of *il-1β* and *il-6* in response to SSC (Jingjiestuitan) extract was measured by RT-qPCR. *Il-1β* expression in LPS-injected larvae showed an immediate response, with a 12-fold increase over the control group, while DEX, and three doses of SSC (Jingjiesuitan) extract markedly reduced *il-1β* levels (Fig. 4J). Similarly, LPS-injection elevated *il-6* mRNA levels, which were subsequently reduced by DEX, as well as medium-dose (1000 μg/mL) and high-dose (2000 μg/mL) of SSC (Jingjiesuitan) extract (Fig. 4J). These results indicate that SSC (Jingjiesuitan) extract effectively mitigates LPS-induced inflammatory responses in vivo.

To further explore compounds that contribute to the anti-inflammatory activity of SSC (Jingjiesuitan), we thereafter performed molecular docking-based virtual screening. The potential of compounds to bind with IKKβ was scored by the binding energy. A lower negative binding energy indicates greater binding potential between the compound and the protein. The top 5 potential compounds in SSC that target IKKβ were isoquercetin, rosmarinic acid, luteolin, quercetin, and diosmetin (Fig. 4K). Then in vitro cell-free enzymatic assays were performed to verify their effects on IKKβ kinase activity. Luteolin was found to inhibit IKKβ activity with an IC50 of 21.232 μM (Fig. 4L). Quercetin reduced IKKβ activity by approximately 46% at 100 μM (Fig. S2C), while isoquercetin (data presented in another paper under

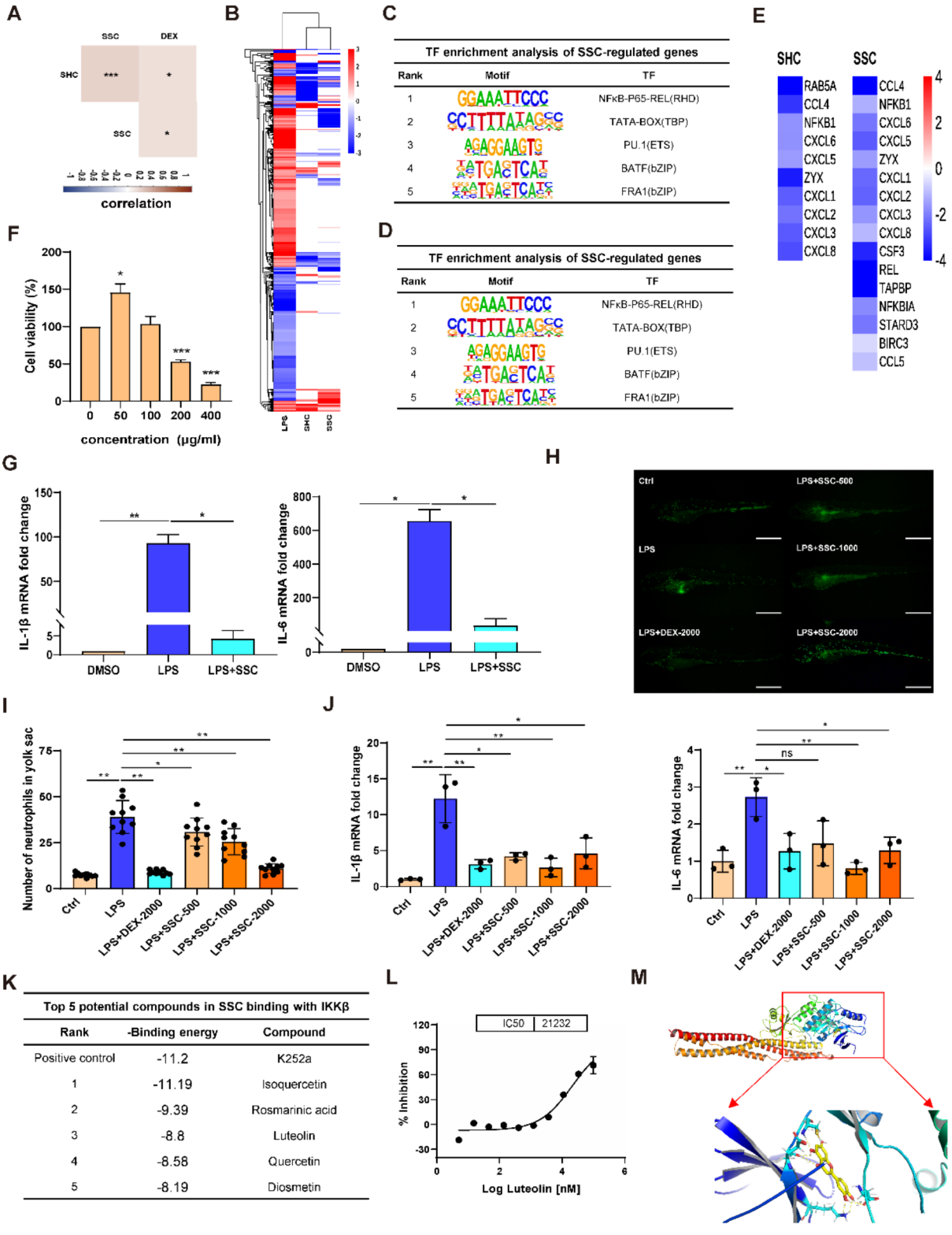
A
SSC
DEX
SHC
SSC
correlation
B
LPS
SHC
SSC
C
TF enrichment analysis of SSC-regulated genes
Rank Motif TF
1 NFκB-P65-REL(RHD)
2 TATA-BOX(TBP)
3 PU.1(ETS)
4 BATF(bZIP)
5 FRA1(bZIP)
D
TF enrichment analysis of SSC-regulated genes
Rank Motif TF
1 NFκB-P65-REL(RHD)
2 TATA-BOX(TBP)
3 PU.1(ETS)
4 BATF(bZIP)
5 FRA1(bZIP)
E
SHC
SSC
RAB5A
CCL4
NFKB1
CXCL6
CXCL5
ZYX
CXCL1
CXCL2
CXCL3
CXCL8
CCL4
NFKB1
CXCL6
CXCL5
ZYX
CXCL1
CXCL2
CXCL3
CXCL8
CSF3
REL
TAPBP
NFKBIA
STARD3
BIRC3
CCL5
F
Cell viability (%)
concentration (μg/ml)
G
IL-1β mRNA fold change
IL-6 mRNA fold change
DMSO
LPS
LPS+SSC
H
Ctrl
LPS
LPS+DEX-2000
LPS+SSC-500
LPS+SSC-1000
LPS+SSC-2000
I
Number of neutrophils in yolk sac
J
IL-1β mRNA fold change
IL-6 mRNA fold change
ns
K
Top 5 potential compounds in SSC binding with IKKβ
Rank -Binding energy Compound
Positive control -11.2 K252a
1 -11.19 Isoquercetin
2 -9.39 Rosmarinic acid
3 -8.8 Luteolin
4 -8.58 Quercetin
5 -8.19 Diosmetin
L
IC50 21232
% Inhibition
Log Luteolin [nM]
M

Fig. 4 Evaluation and validation of the anti-inflammatory activities of *Schizonepetae Spica Carbonisata*. **A** Pearson correlation analysis of the gene signatures of SHC and SSC. **B** Heatmap representing the expression of DEGs induced by LPS in THP-1 cells treated with SHC and SSC extract. **C** TF enrichment analysis of SHC and **D** SSC extract-regulated genes. **E** Heatmap representing the expression of NF-κB downstream genes in THP-1 cells treated with SHC and SSC extract. Red: up-regulated; blue: down-regulated. **F** Cell viability of RAW264.7 cells in response to treatment with different doses of SSC extract. Dose-dependence was analyzed via linear regression analysis. **G** RT–qPCR validation of the relative mRNA levels of *Il-1β* and *Il-6* after treatment with SSC extract in RAW264.7 cells. **H** Typical images of neutrophil recruitment, and **I** neutrophil numbers of inflammatory site of zebrafish after treatment with DEX or SSC extract in LPS-stimulated zebrafish. Magnification: 400X. Scale bar: 600 μm. Dose-dependence was analyzed via linear regression analysis. **J** RT–qPCR validation of the relative mRNA levels of *il-1β* and *il-6* after treatment with DEX or SSC extract in LPS-stimulated zebrafish. **K** Molecular docking scoring of compounds in SSC with IKKβ structure. **L** Effect of luteolin on IKKβ activity. **M** Diagram of the computational docking between luoteolin and IKKβ (PDB ID: 4KIK). $*p < 0.05$; $**p < 0.01$; ns: not significant. DEX: dexamethasone; SHC: Jingjietan, *Schizonepetae Herba Carbonisata*; SSC: Jingjiesuita, *Schizonepetae Spica Carbonisata*

submission), rosmarinic acid, and diosmetin exhibited minimal inhibitory effect on IKKβ activity (Fig. S2C). Further computational docking simulation analysis revealed that luteolin formed direct interactions with IKKβ at Cys99, Lys44, Asp166, and Glu97 (Fig. 4M). These results suggest that luteolin is a major bioactive IKKβ inhibitor in SSC to mediate its anti-inflammatory activity.

In summary, we constructed a large-scale pharmaco-transcriptomic dataset for TCMs and proposed a universal and reliable gene signature-based strategy for the high-throughput screening of anti-inflammatory drugs that is applicable not only to compound screening but also to TCM herbs and TCM formulae. Moreover, we developed a workflow from drug screening to the validation of drug efficacy, elucidation of the mechanism of action, and identification of bioactive compounds (Fig. 5), providing a research template for high-throughput drug research.

Discussion

Inflammation is a protective host response to pathogens and cell or tissue damage that maintains tissue homeostasis and enables an organism to survive during injury or infection [1]. However, excessive or chronic inflammation can have negative effects, leading to inflammatory disorders [1]. Therefore, the discovery of anti-inflammatory drugs is crucial for the therapeutic treatment of patients with inflammation-related diseases. TCM is considered a valuable tool for drug discovery and has excellent potential for the prevention and treatment of various diseases, including inflammatory diseases. After an artemisinin-based remedy for malaria was awarded the Nobel Prize in 2015, TCM has attracted increasing amounts of attention. Research on TCM has entered a new era in the wake of the development of bioinformatics and other approaches, including network pharmacology, proteomics, and metabolomics. However, TCM-based computational drug discovery approaches have not yet been fully utilized, and the mechanisms and bioactive ingredients underlying the effects of TCMs have not been fully elucidated.

With the emergence of high-throughput technologies, gene signature-based methods have been widely used for screening drugs and identifying the molecular action of drugs, including modern medicines and TCMs [13]. CMAP is a large-scale pharmaco-transcriptomic database, containing thousands of well-annotated compounds, and has been widely applied in gene signature-based drug discovery, drug repurposing, and the elucidation of the molecular mechanisms of drugs [13]. To determine the bioactive ingredients in TCMs, Lv et al. constructed a transcriptomic database of 102 TCM active ingredients in 2019 [37], which has been widely used to screen TCM-derived compounds. More recently, the same group constructed a larger data repository of 496 TCM active ingredients and developed six state-of-the-art signature search methods to screen TCM bioactive ingredients [21]. Yan et al. constructed HIT2.0 as the latest curated dataset focusing on herbal ingredients' targets covering PubMed literatures from 2000 to 2020 [38]. For TCM herbs, the HERB [39] and TMNP [40] databases were developed to analyze the gene expression induced by herbal medicines by collecting various datasets from different sources. However, these platforms contain only a small number of herbs and ingredients. For example, HERB comprises only transcriptomic data for 36 herbs and 211 ingredients. Therefore, until recently, high-quality resources for the pharmaco-transcriptomic profiles of TCM herbs have been lacking.

Our group previously established the gene expression profiles of 166 TCM herbs from 125 anti-COVID-19 TCM formulae via high-throughput RASL-seq to evaluate the efficacy of these TCM formulae [16]. In the present study, using the same platform, we performed unified high-throughput experiments and constructed the largest set of TCM pharmaco-transcriptomic data comprising 511 TCM herbs, 49 TCM formulae and 36 TCM ingredients. Moreover, gene signature-based anti-inflammatory drug screening was also performed by comparing the drug gene signatures and disease signatures. First, an LPS-stimulated THP-1 macrophage model was constructed to mimic inflammation, and the disease signature was generated via RNA-seq. High-throughput drug signatures were subsequently obtained using the established RASL-seq platform. Comparisons between disease signatures and drug signatures were

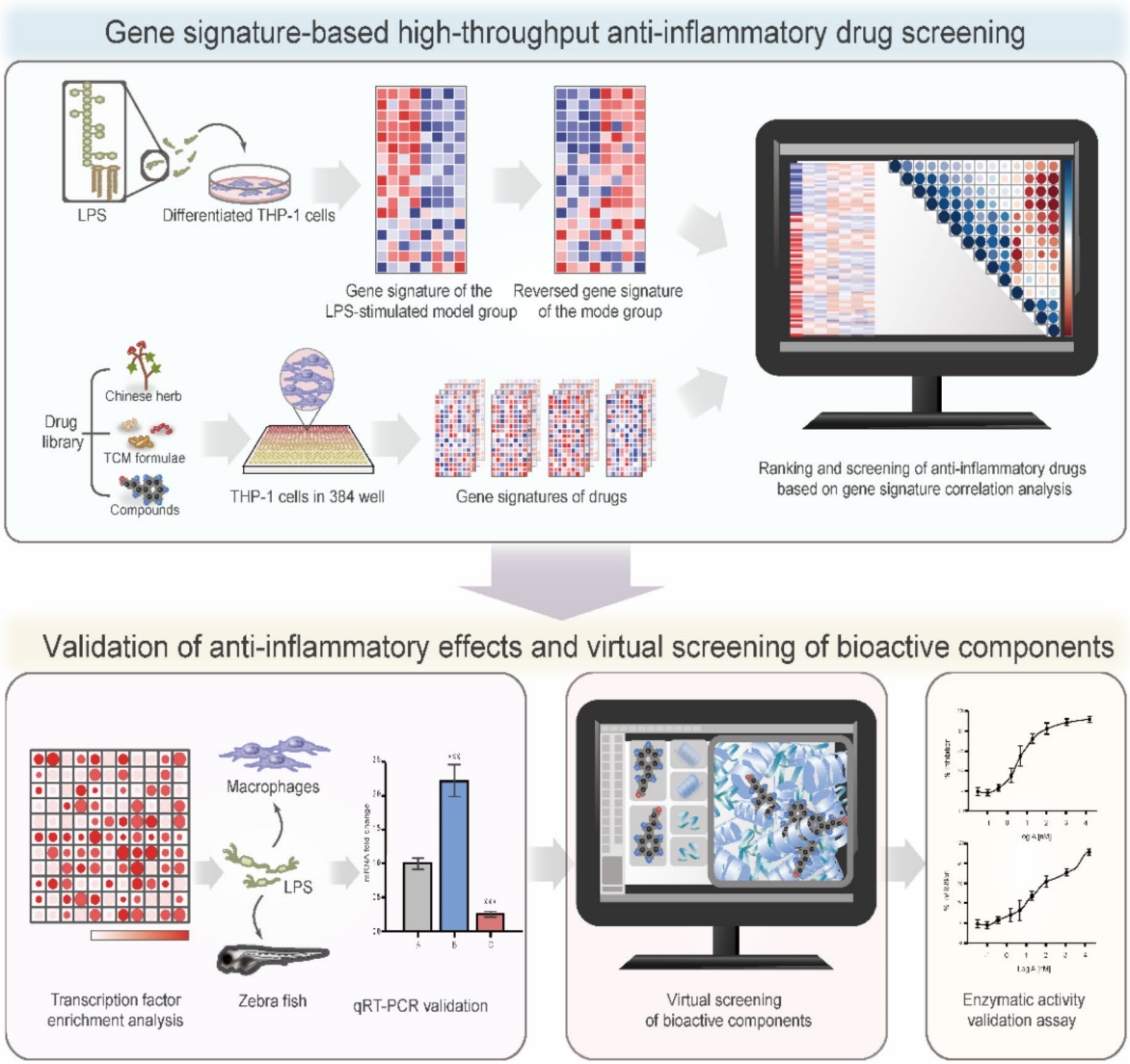

Fig. 5 Schematic flow of gene signature-based high-throughput discovery of anti-inflammatory drugs

subsequently performed via SS_ZhScore analysis. Using this approach, 83 drug candidates were identified to have anti-inflammatory activity, including 10 clinically approved chemical drugs, 7 compounds derived from TCMs, 11 TCM formulae, and 55 TCM herbs, indicating the universality of this method, which could be widely applied for screening compounds, TCM herbs and TCM formulae.

With this strategy, many candidates that has been previously reported to be anti-inflammatory could be effectively screened. For example, the TCM formula BYP (Biyunsan), is commonly used for its purported anti-inflammatory and immunomodulatory effects in rhinitis [41]. CH (Ebushicao) [42, 43], KR (Shannai) [33, 44] and their constituents have been reported to exert anti-inflammatory activities through NF-κB pathway suppression. In our study, their anti-inflammatory activities and inhibitions on NF-κB pathway were verified, thus confirming the reliability of this strategy.

This strategy could also be used to identify new anti-inflammatory drugs, for example, SSC (Jingjiesuitan). SSC (Jingjiesuitan), processed from the spike of the plant *S. tenuifolia* Briq. by stir-frying until carbonization, is commonly used to managing symptoms resembling hemorrhage, such as hematochezia, metrorrhagia and metrostaxis (Chinese Pharmacopoeia, 2020 edition). Compared to the extensive research documenting the anti-inflammatory activity of raw *S. tenuifolia* Briq. extract [34], study claiming the anti-inflammatory activity of SSC was limited. Using the LPS-stimulated RAW264.7 macrophage model, Liu et al. found that 20 μg/mL SSC (Jingjiesuitan) extract

significantly reduced LPS-induced levels of NO and IL-1β but not IL-6 and TNFα [35]. Our study, however, provides a different perspective, showing that SSC (Jingjiesuitan) extract reverted LPS-induced gene signatures via inhibition of NF-κB in THP-1 cells. The anti-inflammatory activity of SSC was further confirmed through both in vitro and in vivo experiments. Our findings demonstrate that SSC (Jingjiesuitan) extract significantly inhibits LPS-stimulated *Il-1β* and *Il-6* expression in both RAW264.7 cells and zebrafish models. The observed more potent anti-inflammatory effect in vitro may be attributed to the higher dose of SSC (Jingjiesuitan) (100 μg/mL) used in our experiments. Lastly, luteolin was identified as an IKKβ inhibitor in SSC (Jingjiesuitan) that contributes its anti-inflammatory activities. Overall, our study provides further theoretical basis for extensive application of SSC (Jingjiesuitan) in anti-inflammation therapy.

In summary, we constructed a large-scale comprehensive TCM pharmaco-transcriptomic dataset and proposed a novel gene signature-based high-throughput drug screening strategy for anti-inflammatory drugs. The advantages of this strategy include the following: (**1**) it is reliable, as many clinically approved anti-inflammatory drugs can be screened using this method; (**2**) this approach is suitable for screening new anti-inflammatory TCMs; (**3**) the major bioactive herbs in TCM formulae or bioactive compounds in TCMs can be identified; and (**4**) the mechanism of action of the screened drugs can be elucidated. Overall, we established a universal strategy for the discovery of anti-inflammatory drugs. Also, our study provides a feasible and comprehensive research template for high-throughput drug research from screening to validation and to the identification of the mechanism of action and active components, which could be expanded to drug discovery for other complicated diseases lacking effective therapeutics. The main limitation of the present study is that the anti-inflammatory activities of the screened drug candidates need more validation with other animal models and even clinical trials in the future to verify the reliability of the strategy.

In conclusion, we constructed a large-scale comprehensive transcriptome dataset for TCMs and established a novel high-throughput gene expression signature-based approach to screen for anti-inflammatory drugs; this approach is not limited to compounds but also applicable to TCM screening. TF enrichment and RT–qPCR analyses were subsequently used to validate the efficacy and mechanism of action of the selected drugs. Enzymatic activity assays were also conducted to validate the bioactive ingredients in TCM herbs underlying their anti-inflammatory effects. Overall, our study provides a novel and effective research template for drug discovery, especially for the research of TCM herbs, and this approach could be expanded to drug discovery for other complicated diseases lacking effective therapeutics.

Supplementary Information The online version contains supplementary material available at https://doi.org/10.1007/s00011-024-01968-4.

Author contributions Juan Feng: Data curation, Formal analysis, Funding acquisition. Writing– original draft, Writing– review & editing. Xiaoling Zhang: Methodology. Honglei Dang, Wenting Huang, Chengmei Ma, Mimi Hao: Validation. Xiaoling Zhang, Aixiang Zhang: Formal analysis. Lan Xie: Resources, Supervision, Writing–review & editing.

Funding This work was supported by the Innovation Team and Talents Cultivation Program of the National Administration of Traditional Chinese Medicine (NO. ZYYCXTD-D-202201); the National Natural Science Foundation of China (NO. 82204759); and the Shenzhen Science and Technology Program (No. JCYJ20240813113239051 & NO. RCBS20210609103650047).

Data availability The datasets for this work are available from the authors upon request.

Declarations

Competing interests The authors declare no competing interests.

References

1. Chovatiya R, Medzhitov R. Stress, inflammation, and defense of homeostasis. Mol Cell. 2014;54:281–8.
2. Ricordi C, Garcia-Contreras M, Farnetti S. Diet and inflammation: possible effects on immunity, chronic diseases, and life span. J Am Coll Nutr. 2015;34(Suppl 1):10–3.
3. Arulselvan P, Fard MT, Tan WS, Gothai S, Fakurazi S, Norhaizan ME et al. Role of antioxidants and natural products in inflammation. Oxid Med Cell Longev. 2016; 2016:5276130.
4. Feng J, Ge C, Li W, Li R. 3-(3-Hydroxyphenyl)propionic acid, a microbial metabolite of quercetin, inhibits monocyte binding to endothelial cells via modulating E-selectin expression. Fitoterapia. 2022;156:105071.
5. Wang X, Wang Q, Li W, Zhang Q, Jiang Y, Guo D, et al. TFEB-NF-kappaB inflammatory signaling axis: a novel therapeutic pathway of dihydrotanshinone I in doxorubicin-induced cardiotoxicity. J Exp Clin Cancer Res. 2020;39:93.
6. Ito K, Caramori G, Adcock IM. Therapeutic potential of phosphatidylinositol 3-kinase inhibitors in inflammatory respiratory disease. J Pharmacol Exp Ther. 2007;321:1–8.

7. Mewar D, Wilson AG. Treatment of rheumatoid arthritis with tumour necrosis factor inhibitors. Br J Pharmacol. 2011;162:785–91.
8. van Dai TVL, van de Vijver H, He MJ, Hart YD, Mao AA. Gene expression profiling predicts clinical outcome of breast cancer. Nature. 2002;415:530–6.
9. Ayers M, Symmans WF, Stec J, Damokosh AI, Clark E, Hess K, et al. Gene expression profiles predict complete pathologic response to neoadjuvant paclitaxel and fluorouracil, doxorubicin, and cyclophosphamide chemotherapy in breast cancer. J Clin Oncol. 2004;22:2284–93.
10. Iorio F, Bosotti R, Scacheri E, Belcastro V, Mithbaokar P, Ferriero R, et al. Discovery of drug mode of action and drug repositioning from transcriptional responses. Proc Natl Acad Sci USA. 2010;107:14621–6.
11. Feng J, Li H, Zhao W, Dang H, Wang R, Luo K, et al. Biological-profiling-based systematic analysis of rhizoma coptidis from different growing regions and its anticholesterol biosynthesis activity on HepG2 cells. Mol Pharm. 2018;15:2234–45.
12. Lee J, Liu J, Feng X, Salazar HM, Mucka P, Ibi D, et al. Withaferin A is a leptin sensitizer with strong antidiabetic properties in mice. Nat Med. 2016;22:1023–32.
13. Huang L, Yi X, Yu X, Wang Y, Zhang C, Qin L, et al. High-throughput strategies for the discovery of anticancer drugs by targeting transcriptional reprogramming. Front Oncol. 2021;11:762023.
14. Li H, Zhou H, Wang D, Qiu J, Zhou Y, Li X, et al. Versatile pathway-centric approach based on high-throughput sequencing to anticancer drug discovery. Proc Natl Acad Sci USA. 2012;109:4609–14.
15. Dai Y, Qiang W, Gui Y, Tan X, Pei T, Lin K, et al. A large-scale transcriptional study reveals inhibition of COVID-19 related cytokine storm by traditional Chinese medicines. Sci Bull (Beijing). 2021;66:884–8.
16. Qiao L, Huang W, Zhang X, Guo H, Wang D, Feng Q, et al. Evaluation of the immunomodulatory effects of anti-COVID-19 TCM formulae by multiple virus-related pathways. Signal Transduct Target Ther. 2021;6:50.
17. Dai Y, Qiang W, Yu X, Cai S, Lin K, Xie L, et al. Guizhi Fuling Decoction inhibiting the PI3K and MAPK pathways in breast cancer cells revealed by HTS(2) technology and systems pharmacology. Comput Struct Biotechnol J. 2020;18:1121–36.
18. Luo K, Huang W, Qiao L, Zhang X, Yan D, Ning Z, et al. Dendrocalamus latiflorus and its component rutin exhibit glucose-lowering activities by inhibiting hepatic glucose production via AKT activation. Acta Pharm Sin B. 2022;12:2239–51.
19. Qiao LS, Li J, Xie L, et al. The exploration of a new approach for developing innovative Chinese herbal formulae by combining targeted transcriptome, expert experience and artificial intelligence: taking the development of antichronic heart failure innovative formula as an example. J Tradit Chin Med. 2023;64(03):217–24. (Chinese).
20. Zhang SD, Gant TW. A simple and robust method for connecting small-molecule drugs using gene-expression signatures. BMC Bioinform. 2008;9:258.
21. Tian S, Zhang J, Yuan S, Wang Q, Lv C, Wang J et al. Exploring pharmacological active ingredients of traditional Chinese medicine by pharmacotranscriptomic map in ITCM. Brief Bioinform 2023; 24.
22. Lill MA, Danielson ML. Computer-aided drug design platform using PyMOL. J Comput Aided Mol Des. 2011;25:13–9.
23. Wang H, Huang W, Liang M, Shi Y, Zhang C, Li Q, et al. (+)-JQ1 attenuated LPS-induced microglial inflammation via MAPK/NFkappaB signaling. Cell Biosci. 2018;8:60.
24. Do CH, Lee DH. Synergism between taurine and dexamethasone in anti-inflammatory response in lps-activated macrophages. Adv Exp Med Biol. 2022;1370:31–9.
25. Horby P, Lim WS, Emberson JR, Mafham M, Bell JL, Linsell L, et al. Dexamethasone in hospitalized patients with Covid-19. N Engl J Med. 2021;384:693–704.
26. Bousquet J. Mometasone furoate: an effective anti-inflammatory with a well-defined safety and tolerability profile in the treatment of asthma. Int J Clin Pract. 2009;63:806–19.
27. Alam W, Khan H, Shah MA, Cauli O, Saso L. Kaempferol as a dietary anti-inflammatory agent: current therapeutic standing. Molecules 2020; 25.
28. He D, Fu S, Zhou A, Su Y, Gao X, Zhang Y, et al. Camptothecin regulates microglia polarization and exerts neuroprotective effects via activating akt/nrf2/ho-1 and inhibiting nf-kappab pathways in vivo and in vitro. Front Immunol. 2021;12:619761.
29. Hong S, Dia VP, Zhong Q. Synergistic anti-inflammatory activity of apigenin and curcumin co-encapsulated in caseins assessed with lipopolysaccharide-stimulated RAW 264.7 macrophages. Int J Biol Macromol. 2021;193:702–12.
30. Meng T, Xiao D, Muhammed A, Deng J, Chen L, He J. Anti-inflammatory action and mechanisms of resveratrol. Molecules 2021; 26.
31. Wang LL, Sun Y, Huang K, Zheng L. Curcumin, a potential therapeutic candidate for retinal diseases. Mol Nutr Food Res. 2013;57:1557–68.
32. Jia W, He X, Jin W, Gu J, Yu S, He J, et al. Ramulus Cinnamomi essential oil exerts an anti-inflammatory effect on RAW264.7 cells through N-acylethanolamine acid amidase inhibition. J Ethnopharmacol. 2023;317:116747.
33. Kumar A. Phytochemistry, pharmacological activities and uses of traditional medicinal plant Kaempferia galanga L.—An overview. J Ethnopharmacol. 2020;253:112667.
34. Zhao X, Zhou M. Review on chemical constituents of Schizonepeta Tenuifolia Briq. And their pharmacological effects. Molecules 2022; 27.
35. Liu X, Huang Z, Zhang J, Zhou Y, Zhang Y, Wu M, et al. Comparisons of the anti-inflammatory, antiviral, and hemostatic activities and chemical profiles of raw and charred Schizonepetae Spica. J Ethnopharmacol. 2021;278:114275.
36. Yang LL, Wang GQ, Yang LM, Huang ZB, Zhang WQ, Yu LZ. Endotoxin molecule lipopolysaccharide-induced zebrafish inflammation model: a novel screening method for anti-inflammatory drugs. Molecules. 2014;19:2390–409.
37. Lv C, Wu X, Wang X, Su J, Zeng H, Zhao J, et al. The gene expression profiles in response to 102 traditional Chinese medicine (TCM) components: a general template for research on TCMs. Sci Rep. 2017;7:352.
38. Yan D, Zheng G, Wang C, Chen Z, Mao T, Gao J, et al. HIT 2.0: an enhanced platform for herbal ingredients' targets. Nucleic Acids Res. 2022;50:D1238–43.
39. Fang S, Dong L, Liu L, Guo J, Zhao L, Zhang J, et al. HERB: a high-throughput experiment- and reference-guided database of traditional Chinese medicine. Nucleic Acids Res. 2021;49:D1197–206.
40. Li P, Zhang H, Zhang W, Zhang Y, Zhan L, Wang N et al. TMNP: a transcriptome-based multi-scale network pharmacology platform for herbal medicine. Brief Bioinform 2022; 23.
41. Huang ZT, Huang TT. Treatment of allergic rhinitis with Yufeng Hubi cecoction combined with Biyun powder: a study of 84 cases. J Sichuan Tradit Chin Med. 2010;28(07):109–10. (Chinese).
42. Li SY, Zhou YL, He DH, Liu W, Fan XZ, Wang Q, et al. Centipeda minima extract exerts antineuroinflammatory effects via the inhibition of NF-kappaB signaling pathway. Phytomedicine. 2020;67:153164.
43. Tan J, Qiao Z, Meng M, Zhang F, Kwan HY, Zhong K, et al. Centipeda minima: an update on its phytochemistry, pharmacology and safety. J Ethnopharmacol. 2022;292:115027.

44. Tarasuk M, Songprakhon P, Muhamad P, Panya A, Sattayawat P, Yenchitsomanus PT. Dual action effects of ethyl-p-methoxycinnamate against dengue virus infection and inflammation via NF-kappaB pathway suppression. Sci Rep. 2024;14:9322.